# LOAD CARRYING BEHAVIOUR OF THRUST RINGS

R. Ofner, R. Greiner

Abstract: The design of thrust rings for the axial anchorage of penstocks may be carried out on the assumption of different pressure distributions between the ring and the surrounding concrete. This results in a different design. In this paper the load carrying behaviour of thrust rings is presented on the basis of FE-results. Finally a concept for the design of thrust rings with a more realistic pressure distribution between the ring and the concrete is proposed.

## 1 Introduction

Penstocks for hydro power plants have to be anchored at certain places to transmit axial forces into the surrounding concrete. This anchorage is carried out by thrust rings. They are often made of flat steel plates. For the design of these rings two different pressure distributions between the ring and the concrete may be assumed (Fig.1). On the one hand the pressure distribution results in a clamped restraint of the ring into the pipe (1) and on the other hand the pressure distribution results in a clamped restraint of the ring into the surrounding concrete (2). The load carrying capacity of the thrust ring are $N_{Rd,1}=0.67\cdot\sigma_{c,1}\cdot h$ respectively $N_{Rd,2}=0.25\cdot\sigma_{c,2}\cdot h$.

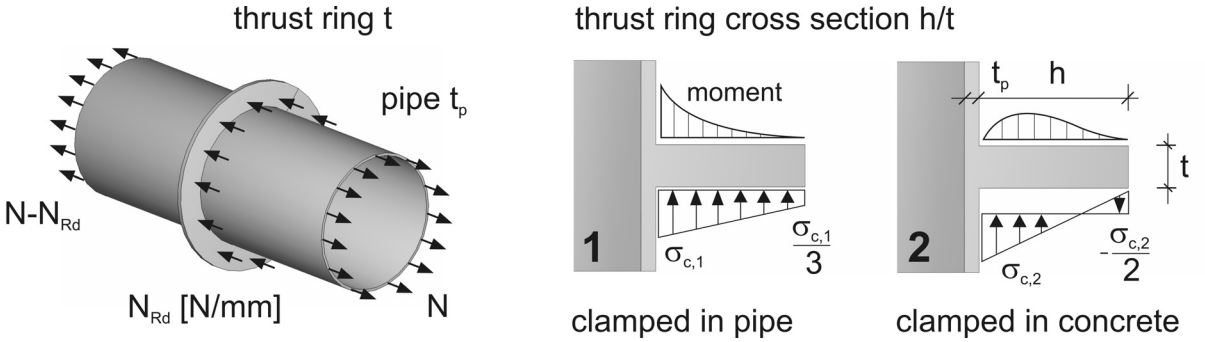


Fig.1 Thrust ring with different assumptions for the contact pressure distribution

These different assumptions lead to a different design of the thrust rings. There is no rule which pressure distribution should be used, e.g. in relation to the height over thickness ratio h/t of the ring or in relation to the ratio of the thickness of the pipe to the thickness of the ring $t_p/t$. The choice of the pressure distribution, therefore, is rather randomly selected. To find out which pressure distribution should be used for the design some different configurations have been investigated.

## 2 Results of the investigation

The load carrying behaviour of thrust rings made of flat steel plates are investigated on the basis of the Finite Element Method with ABAQUS [5]. The axisymmetric solid FE-models include - among other parameters - the contact behaviour between the pipe and the concrete. For the contact no friction is assumed. The material behaviour of the concrete is defined by a parabolic stress-strain curve according to [1] but without a crack model.

The first investigation concerns the distribution of the axial force if several thrust rings are arranged in a row (Fig.2). In this example the ratio of the mean value to the highest ring force $\beta_{Lf}$ is 0.62. This means that the design of thrust rings can be on the unsafe side if the axial force is distributed evenly in a row of thrust rings.

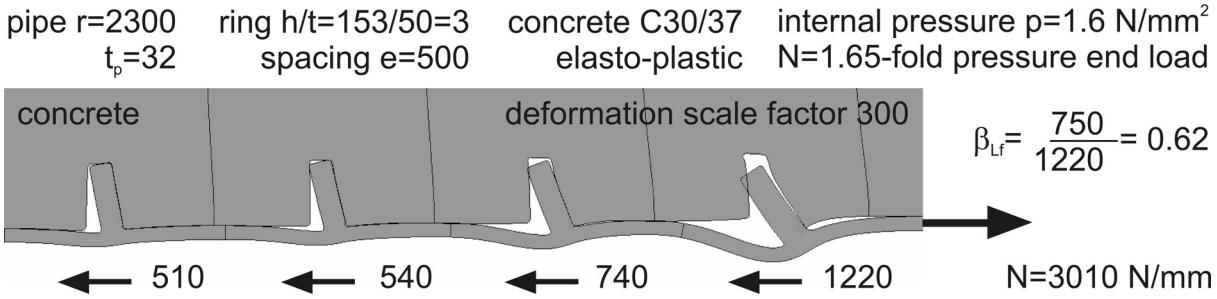


Fig.2 Uneven distribution of the axial force for thrust rings in a row

This effect is also known from long bolted connections. There a reduction factor $\beta_{Lf}$ for the shear resistance of the bolt is introduced [2]. The reduction factor is in between 1.0 and 0.75. This rule can be the basis for an adaptation to a row of thrust rings. There are additional parameters which influence the uneven loading, e.g. the more complex geometry, the concrete and the contact behaviour. For a general conclusion further investigations are necessary to determine important parameters and their effects.

The next investigation concerns the load carrying behaviour of a single thrust ring. The aim is to find out a realistic pressure distribution between the ring and the concrete. Four configurations are presented in the following. The first axisymmetric solid FE-model is shown in Fig.3. The ring has an h/t-ratio of 6 and the ratio of the thickness of the pipe to the thickness of the ring $t_p/t$ is 1.2. The design values of the internal pressure ($p=\gamma_F \cdot 11.2=16.8 N/mm^2$) and the axial force ($N-N_{Rd}$) are in accordance with an actual example. N results from the pressure end load. It is obvious that the pressure distribution in Fig.3 is significantly different to the assumptions presented in Fig.1. The contact pressure has approximately the shape of a triangle over the half height of the ring and a concentrated contact force K at the outer edge of the ring.
A variation of this example is carried out for an axial force $N=N_{Rd}=2100 N/mm$ and therefore $(N-N_{Rd})=0$. This result as well in a triangular contact pressure over the half height of the ring and a comparable concentrated contact force K but the MISES stress at the inner surface of the pipe is reduced from $370 N/mm^2$ to $300 N/mm^2$ and the value at the fillet increased from $330 N/mm^2$ to $400 N/mm^2$.

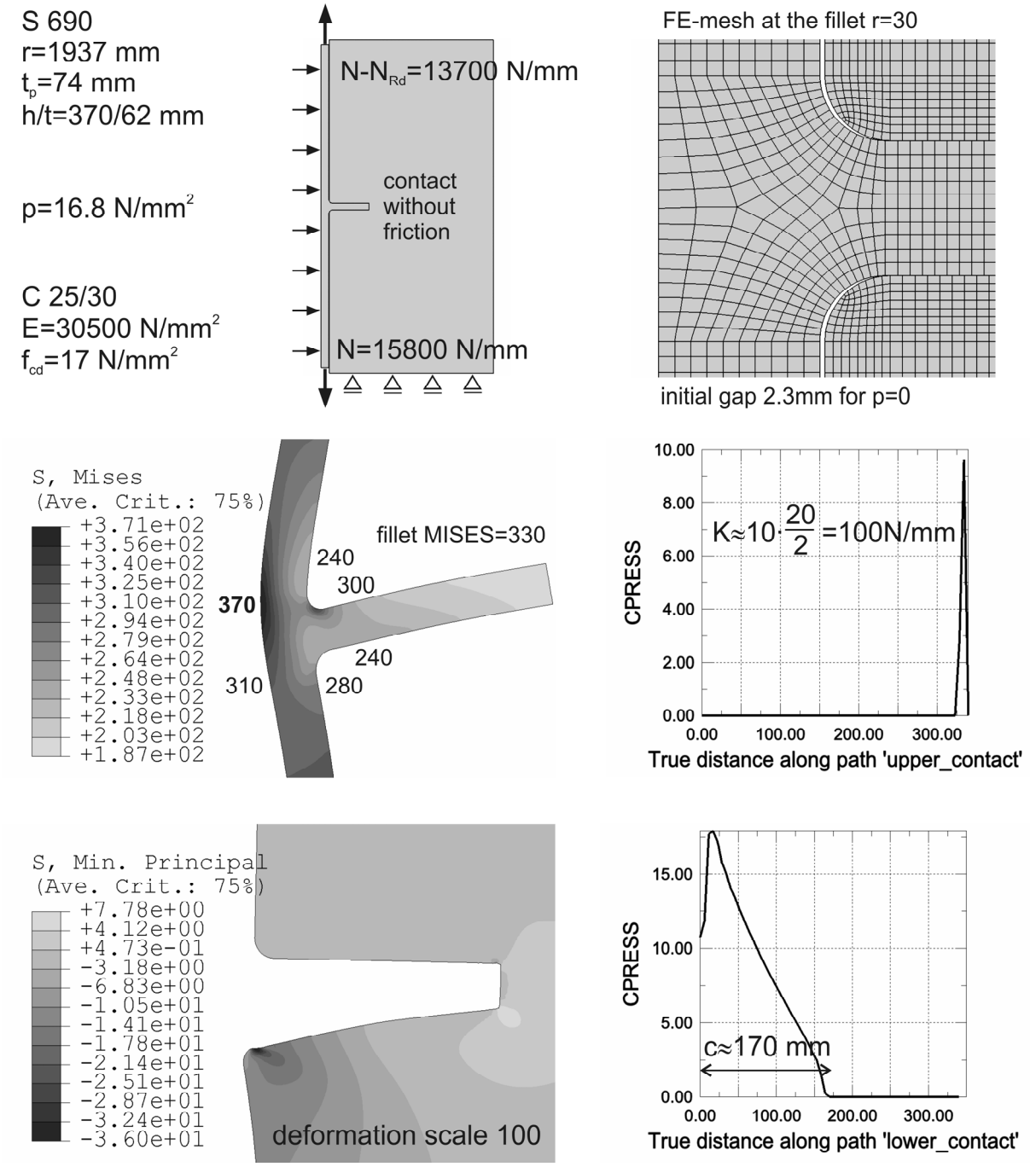


Fig.3 Contact pressure CPRESS [N/mm²] of a thrust ring h/t=370/62, pipe $t_p$=74mm

In order to estimate the influence of the h/t-ratio a further geometry is analysed (Fig.4). Now the ring has an h/t-ratio of 3 and the $t_p$/t-ratio is 1.2 again. The internal pressure and the axial force is the same as in Fig.3. The shape of the contact pressure is triangular as before and also the length of the contact is comparable. This means that the length of the contact is not so much in relation to the height of the ring but more in relation to the thickness of the ring. Unlike the geometry before the concentrated contact force K at the outer edge of the ring vanishes. This effect is supported by the rather high $t_p$/t-ratio.

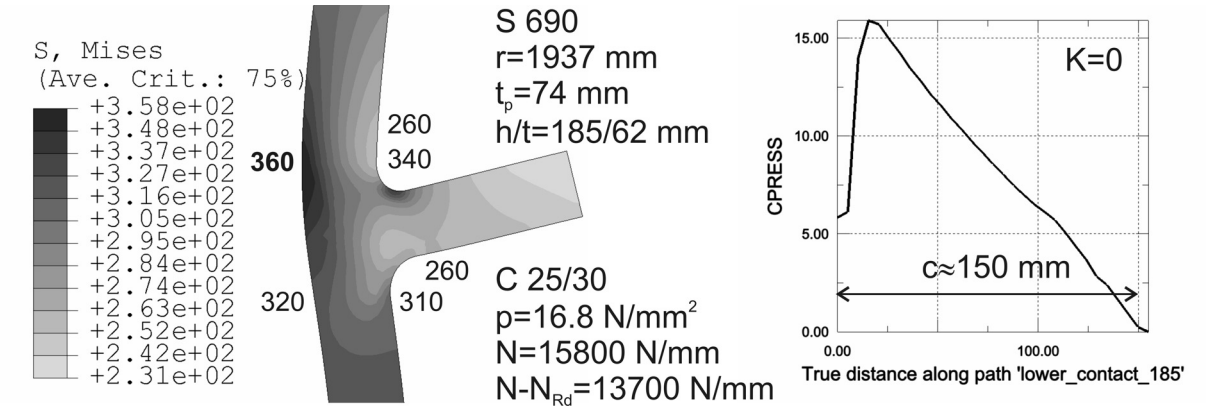


Fig.4 Contact pressure CPRESS [N/mm$^2$] of a thrust ring h/t=185/62, pipe $t_p$=74mm

The next variation of the geometry is show in Fig.5. The h/t-ratio of the ring is 6 but now the $t_p$/t-ratio is 0.6. The internal pressure p and the axial force N are halved but $N_{Rd}$ is defined as before. The contact pressure remains triangular over a length of about 150mm and as expected the concentrated contact force K increases due to the lower clamping effect of the ring into the pipe.
An analysis with a linear elastic material behaviour of the concrete results in a peak contact pressure at the fillet which is four times higher than the peak contact pressure with the elasto-plastic material behaviour. The length of the contact is halved.

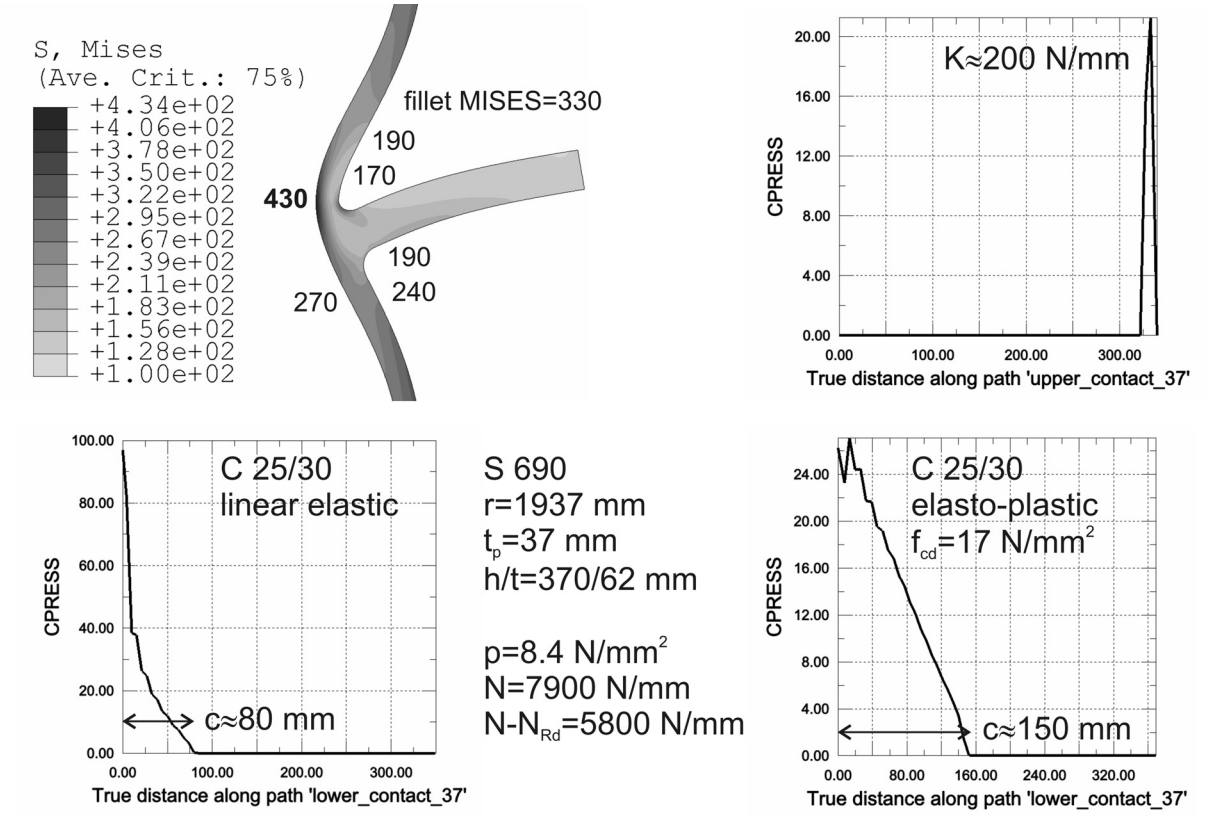


Fig.5 Contact pressure CPRESS [N/mm$^2$] of a thrust ring h/t=370/62, pipe $t_p$=37mm

An extreme variation of the geometry is presented in Fig.6. The h/t-ratio of the ring is 12 and the $t_p$/t-ratio is 0.6 again. As before the contact pressure is triangular but the length of the contact is reduced to about 120mm. The concentrated contact force decreases in comparison with the example in Fig. 5 however the length of the lever arm is twice as before. The result of the linear elastic analysis shows a significantly reduced length of the contact as already mentioned for the example in Fig.5. Further the contact at the upper surface indicates a low contact pressure over a length of about 130mm. The concentrated contact force K at the outer edge still remains there due to the reduced deformation of the concrete at the edge.

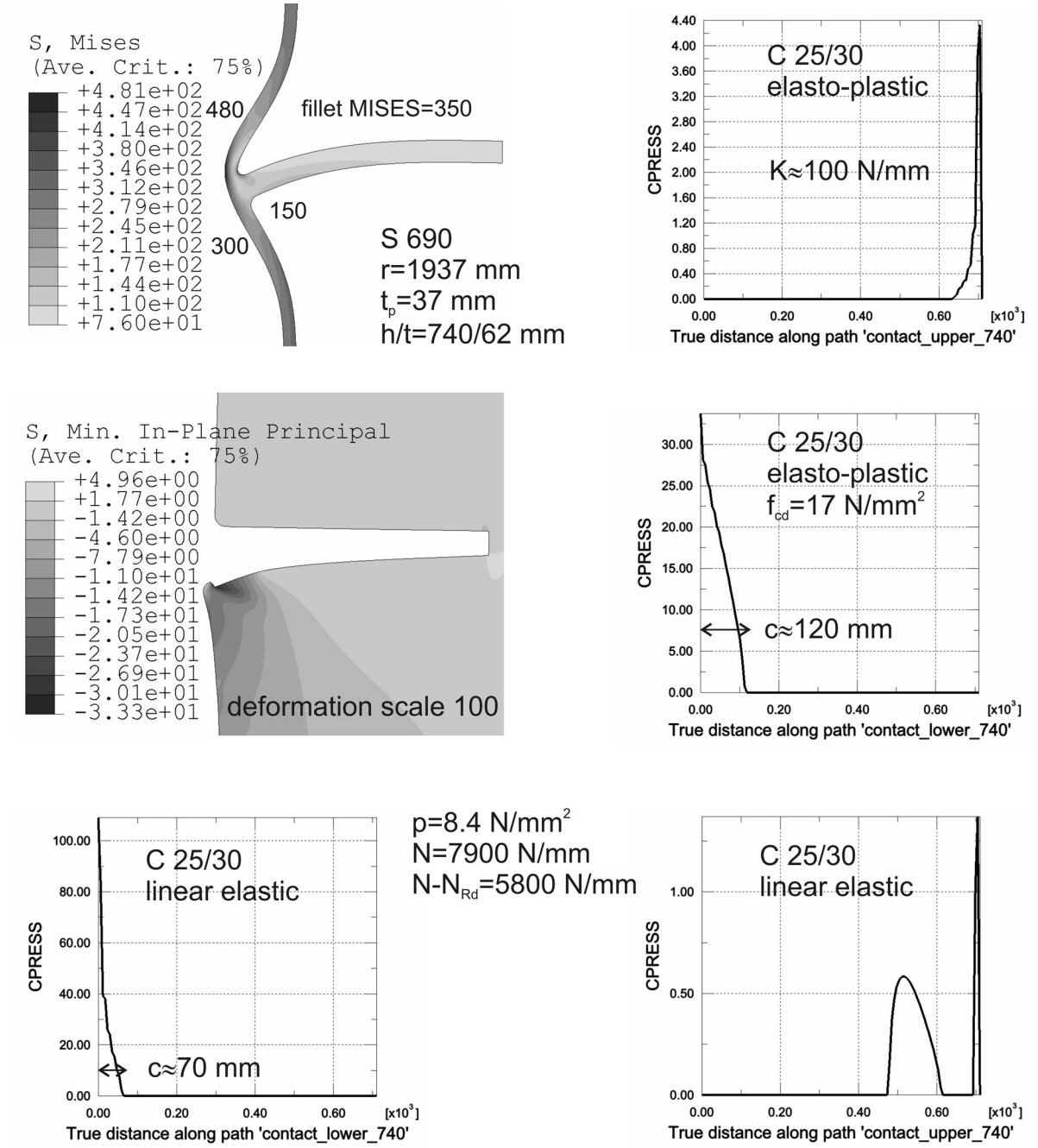


Fig.6 Contact pressure CPRESS [N/mm²] of a thrust ring h/t=740/62, pipe $t_p$=37mm

The parameter variations have shown that the concentrated contact force K can drop down to zero but the shape of the contact pressure remains approximately a triangle over a length which does not correspond with the height of the ring. A conclusion for the design of a thrust ring with a flat plate can be found by predefining an h/t-ratio of about 4 to 6. A lower ratio will hardly activate a clamping effect into the concrete and this can be unfavourable for the pipe. A higher ratio will hardly increase the load carrying capacity of the ring because the contact length depends mainly on the thickness of the ring and not on the height of the ring. In chapter 3 a formula will be proposed for the h/t-ratio of the thrust ring.
In addition to the presented results some other parameters have been varied, e.g. the radius of the fillet. This part of the member is of importance due to the high concrete pressure. The reinforcement near the fillet must fulfil the requirements for the local compressive strength of the concrete. Another attention has to be turned on the stress in the steel at the fillet. This stress depends mainly on the fillet radius. The question is how this stress which results from a solid FE-model should be interpreted in respect to the fatigue check (nominal stress or hot spot stress) and to the choice of the detail category. Here is still a lack of experiences and of regulations.

## 3 Proposal for the design of a thrust ring

Finally a proposal is worked out for the design or at least the pre-design of a thrust ring without an FE-analysis. The basis for the mechanical model is the contact pressure distribution presented in chapter 2. This contact pressure distribution and in addition the axial force and the internal pressure are applied on a shell model without contact to a surrounding concrete. Of course, a detailed stress field near the fillet cannot be calculated with a shell model but the advantage is that the member can be calculated by formulae. The arrangement of the mechanical model with its parameters is given in Fig.7.

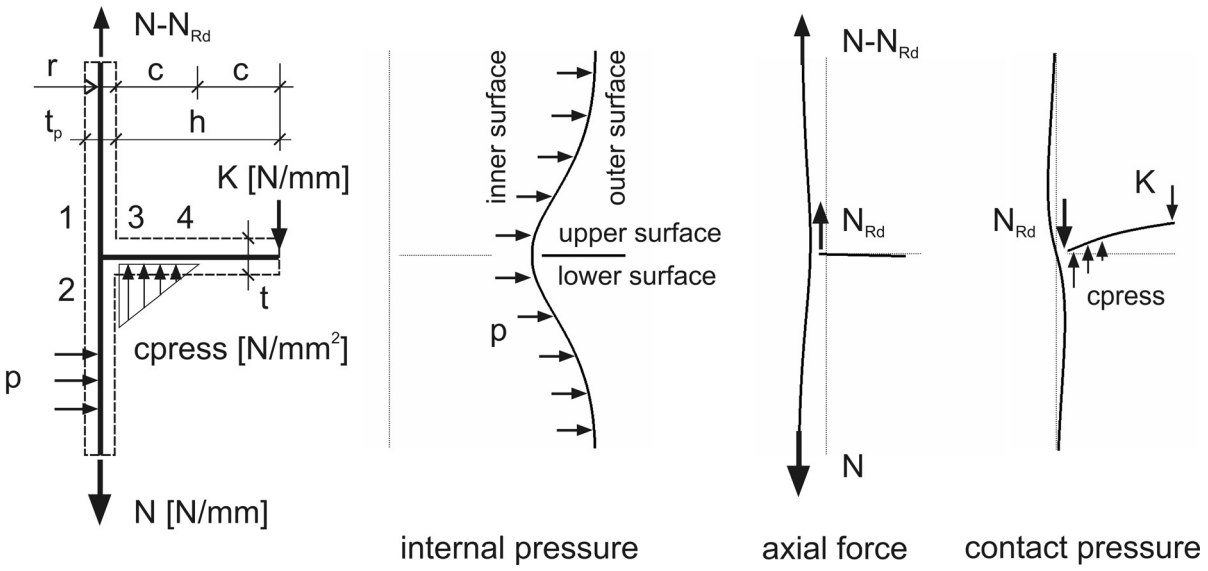


Fig.7 Parameters of the shell model and the loading situation

For the formulae of the proposal some assumptions are necessary. One assumption concerns the strength of the concrete. The local compressive strength $f_{cd,L}$ [N/mm$^2$] is

specified in standards [1] for central loading on a local area $A_L$ which is surrounded by an area A but not for the arrangement of a thrust ring. Nevertheless this specification will be adopted for the thrust ring (Eq.1).

$$f_{cd,L} = \frac{f_{ck}}{\gamma_c} \cdot \sqrt{\frac{A}{A_L}} = \frac{f_{ck}}{1.5} \cdot \sqrt{2} = \sqrt{2} \cdot f_{cd} \qquad (1)$$

The next definition refers to the length c [mm] of the contact pressure. The formula for the length is derived from the following assumption. The stress in the ring near the fillet adds up from the contraction due to the internal pressure and the Poisson effect of the axial force as well as from the bending stress due to the contact pressure (Fig.7). If we assume that the bending stress in the ring due to the contact pressure is limited by $f_{yd}/3$ to give enough space for the other stress components then the length of the contact is determined by Eq.2. The same consideration is applied for the pipe and therefore the minimum of (1 ; $\sqrt{2}\cdot t_p/t$) is added. Thus the length c relates to the thickness of the pipe for a $t_p/t$-ratio less than $1/\sqrt{2}$.
Another predefinition is the height of the thrust ring which is proposed in advance by the fixed value h=2·c (Eq.2). This leads to an h/t-ratio of about 4 to 6. In this proposal only the thickness t of the ring has to be given and the other data, the height h, the capacity $N_{Rd}$ and the MISES stresses, are determined by Eq.1 to Eq.9.

$$c = t \cdot \sqrt{\frac{f_{yd}}{3 \cdot f_{cd,L}}} \cdot \min\left(1\,;\,\sqrt{2}\,\frac{t_p}{t}\right) \qquad \text{and} \qquad h = 2 \cdot c \qquad (2)$$

With some further assumptions for the $K/N_{Rd}$-ratio the resistance $N_{Rd}$ [N/mm] of a single thrust ring is determined by Eq.3. The concentrated contact force K is at the outer edge of the ring and $K_p$ corresponds to the radius of the pipe. A comparison of Eq.2 and Eq.3 with FE-results is given in Tab.1.

$$N_{Rd} = \frac{f_{cd,L} \cdot h}{4} \cdot \frac{1}{1 + \frac{K_p}{N_{Rd}}} \qquad \text{with} \qquad \frac{K_p}{N_{Rd}} = \frac{0.2}{1 + 2 \cdot \left(\frac{t_p}{t}\right)^2} \qquad \text{and} \qquad \frac{K}{N_{Rd}} = \frac{K_p}{N_{Rd}} \cdot \frac{1}{1 + \frac{h}{r}} \qquad (3)$$

| | Fig.3 | Eq.2 and Eq.3 | Fig.5 | Eq.2 and Eq.3 |
|---|---|---|---|---|
| c | 170 | 185 | 150 | 156 |
| $K/N_{Rd}$ | 0.048 | 0.044 | 0.095 | 0.098 |
| $N_{Rd}$ | 2100 | 2070 | 2100 | 1650 |

Tab.1 Comparison of Eq.2 and Eq.3 with Fig.3 and Fig.5

The next set of formulae applies to the calculation of the axial stress $\sigma_x$ and the hoop stress $\sigma_\phi$ at the points 1 to 4 (Fig.7) resulting from the contraction due to the internal pressure p (Eq.5) and due to the axial force N (Eq.6). The sign $\pm$ in Eq.5 and Eq.6 refers to the inner/outer surface. These equations are derived for a cylindrical shell with a radius r and a wall thickness $t_p$. The mechanical model for the ring is not an annular plate but has only a ring area A=h·t. For the stresses due to the axial force the mean value of N and ($N-N_{Rd}$) is used (Eq.4).

$$\kappa = \frac{1}{1+\frac{L_E \cdot t_p}{h \cdot t}} \qquad \text{with} \qquad L_E = 1.56 \cdot \sqrt{r \cdot t_p} + t$$

$$\sigma^p_{\phi 0} = \frac{p \cdot r}{t_p} \qquad \text{respectively} \quad \sigma^N_{\phi 0} = \nu \cdot \frac{N - 0.5 \cdot N_{Rd}}{t_p} \qquad \text{with} \quad \nu = 0.3 \tag{4}$$

$$\sigma^p_{x,1,2} = \pm 1.82 \cdot \kappa \cdot \sigma^p_{\phi 0}$$
$$\sigma^p_{\phi,1,2} = +(1-\kappa) \cdot \sigma^p_{\phi 0} \pm \nu \cdot 1.82 \cdot \kappa \cdot \sigma^p_{\phi 0} \tag{5}$$
$$\sigma^p_{\phi,3,4} = +(1-\kappa) \cdot \sigma^p_{\phi 0} \qquad \text{and} \qquad \sigma^p_{x,3,4} = 0$$

$$\sigma^N_{x,1} = +\frac{N - N_{Rd}}{t_p} \mp 1.82 \cdot \kappa \cdot \sigma^N_{\phi 0} \qquad \text{and} \qquad \sigma^N_{x,2} = +\frac{N}{t_p} \mp 1.82 \cdot \kappa \cdot \sigma^N_{\phi 0}$$
$$\sigma^N_{\phi,1,2} = +\kappa \cdot \sigma^N_{\phi 0} \mp \nu \cdot 1.82 \cdot \kappa \cdot \sigma^N_{\phi 0} \tag{6}$$
$$\sigma^N_{\phi,3,4} = +(\kappa - 1) \cdot \sigma^N_{\phi 0} \qquad \text{and} \qquad \sigma^N_{x,3,4} = 0$$

Eq.8 is used for the calculation of the stresses resulting from the bending moment of the contact pressure and the concentrated contact force. The sign $\pm$ in Eq.8 refers to the inner/outer respectively upper/lower surface. The moments are calculated as if the ring is a cantilever beam (Eq.7). This is obviously a simplification of the annular plate. The difference of the moments resulting from a shell analysis and Eq.7 depends on the h/r-ratio. For an h/r-ratio less than 0.2 the difference of the moments is less than 10%. A shell analysis can be carried out e.g. by [3], [4] or by a software for axisymmetric shells. In an axisymmetric shell analysis K is used whereas $K_p$ is used in Eq.7. The stress $\sigma_\phi$ in Eq.8 comes from the effect of a shell due to $\sigma_x$.

$$M_1 = +\frac{1}{2} \cdot \left[ f_{cd,L} \cdot \frac{h^2}{24} \cdot \left(1 + \frac{3 \cdot t_p}{h}\right) - K_p \cdot h \cdot \left(1 + \frac{t_p}{2 \cdot h}\right) \right] = -M_2$$
$$M_3 = +f_{cd,L} \cdot \frac{h^2}{24} - K_p \cdot h \tag{7}$$
$$M_4 = +f_{cd,L} \cdot \frac{m^3}{3 \cdot h} - K_p \cdot \left(\frac{h}{2} + m\right) \qquad \text{with} \quad m = \sqrt{\frac{K_p \cdot h}{f_{cd,L}}}$$

$$\sigma^M_{x,1,2} = \pm \frac{6 \cdot M_{1,2}}{t_r^2} \qquad \text{and} \qquad \sigma^M_{\phi,1,2} = \nu \cdot \sigma^M_{x,1,2}$$
$$\sigma^M_{x,3,4} = \mp \frac{6 \cdot M_{3,4}}{t^2} \qquad \text{and} \qquad \sigma^M_{\phi,3,4} = \nu \cdot \sigma^M_{x,3,4} \tag{8}$$

The related stresses of Eq.5, Eq.6 and Eq.8 are added up and the verification is done by the MISES stress (Eq.9) for each point i=1 to 4 at both surfaces (Fig.7, Tab.2).

$$\sigma_{MISES,i} = \sqrt{\sigma^2_{x,i} + \sigma^2_{\phi,i} - \sigma_{x,i} \cdot \sigma_{\phi,i}} \le f_{yd} \tag{9}$$

## Example

The data of the example are summarized in Tab.2 (proposal) and in Fig.3 (FEM). The length of the triangular contact pressure according to Eq.2 (185mm) is in a good correlation with the result in Fig.3 (170mm). The difference of the maximum MISES stress between Eq.9 (463N/mm$^2$) and the solid FE-model (370N/mm$^2$) is rather high (25%) but this must be expected due to the significant difference of the two mechanical models and due to the high stress gradients near the fillet. The position of the maximum stress is at the inner surface of the pipe in both models. For a further comparison the result of an accurate shell analysis [5] is given in Tab.2 in the column MISES in italic type (438N/mm$^2$). In the shell analysis the mechanical model of the ring is an eccentrically attached annular plate to a cylindrical shell. The contact pressure distribution is according Fig.7 and Eq.3.

| | **steel** |
|---|---|
| yield stress $f_{yk}$ [N/mm$^2$] | 690 |
| partial factor $\gamma_s$ | 1.1 |
| poisson ratio $\nu$ | 0.3 |
| | **concrete** |
| compression $f_{ck}$ [N/mm$^2$] | 25 |
| partial factor $\gamma_c$ | 1.5 |
| | **load** |
| internal pressure p [N/mm$^2$] | 16.8 |
| axial force N [N/mm] | 15800 |
| partial factor $\gamma_F$ | 1.5 |
| | |
| contact ratio $K_p/N_{Rd}$ | 0.052 |
| **geometry** | **geometry** |
| pipe radius r [mm] | 1937 |
| pipe thickness $t_p$ [mm] | 74 |
| ring thickness t [mm] | **62** |

| **stresses** N/mm$^2$ | | due to p | N | M | Σ | MISES |
|---|---|---|---|---|---|---|
| 1 inside | $\sigma_x$ | 257 | 150 | 94 | 501 | 463 |
| | $\sigma_\phi$ | 376 | 9 | 28 | 412 | *438* |
| 1 outside | $\sigma_x$ | -257 | 220 | -94 | -131 | 310 |
| | $\sigma_\phi$ | 221 | 30 | -28 | 223 | *297* |
| 2 inside | $\sigma_x$ | 257 | 178 | -94 | 342 | 349 |
| | $\sigma_\phi$ | 376 | 9 | -28 | 356 | *346* |
| 2 outside | $\sigma_x$ | -257 | 248 | 94 | 84 | 248 |
| | $\sigma_\phi$ | 221 | 30 | 28 | 279 | *271* |
| 3 upper | $\sigma_x$ | 0 | 0 | -149 | -149 | 315 |
| | $\sigma_\phi$ | 298 | -40 | -44 | 214 | *347* |
| 3 lower | $\sigma_x$ | 0 | 0 | 149 | 149 | 262 |
| | $\sigma_\phi$ | 298 | -40 | 44 | 302 | *266* |
| 4 upper | $\sigma_x$ | 0 | 0 | 36 | 36 | 253 |
| | $\sigma_\phi$ | 298 | -40 | 11 | 269 | *235* |
| 4 lower | $\sigma_x$ | 0 | 0 | -36 | -36 | 267 |
| | $\sigma_\phi$ | 298 | -40 | -11 | 247 | *260* |

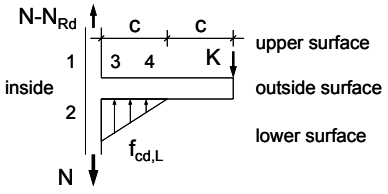


| **result** | |
|---|---|
| contact length c [mm] | 185 |
| ring height h=2c [mm] | **370** |
| ring capacity $N_{Rd}$ [N/mm] | **2069** |

| **result** | | MISES |
|---|---|---|
| pipe | max | 463 |
| ring | max | 314 |
| steel | $f_{yd}$ | 627 |

Tab.2 Input data and results for the example according to the proposal

An outlook for a further concept which provides a higher level of exploitation of the thrust ring capacity is presented in Fig.8. For the example in Fig.3 the reference load (internal pressure and axial force) is increased until the limit state. A limit load factor of 2.3 can be achieved under the condition that the concrete does not crack. The material behaviour of the concrete is defined by a parabolic stress-strain curve according to [1] but without a crack model (a crack model without reinforcement results in a load factor well below 1.0). Fig. 8 presents the state at the load factor of 2.0 (p=2.0·16.8 N/mm$^2$). In the pipe and in the ring distinct plastic zones exist. The length of the contact is 185mm which is comparable with the length at the load factor of 1.0 (Fig.3) but the shape of the contact pressure tends from triangular to parabolic.

In further investigations attention should be turned on the behaviour of the reinforced concrete close to the thrust ring and if a parabolic contact pressure is acceptable.

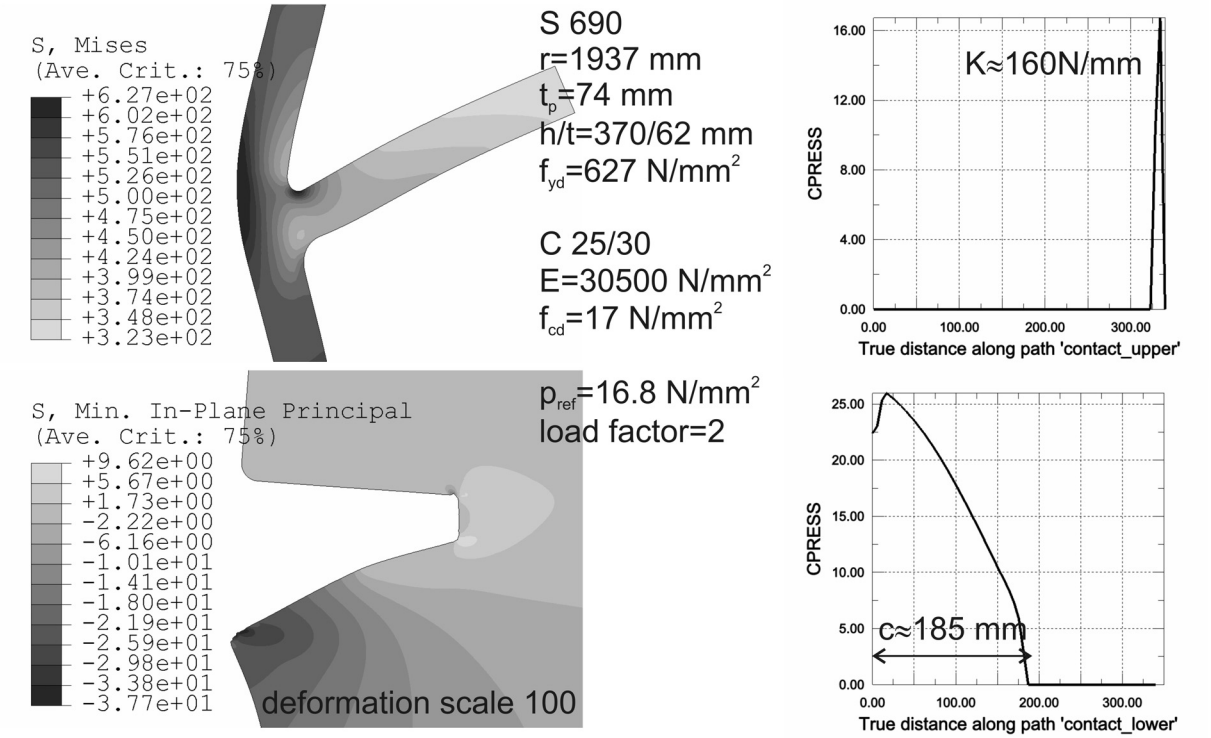


Fig.8 Contact pressure CPRESS [N/mm$^2$] of a thrust ring h/t=370/62, pipe $t_p$=74mm

## Conclusion

The FE-results in chapter 2 provide an inside into the load carrying behaviour of thrust rings. In chapter 3 a concept for the design is proposed. In this proposal only the thickness of the ring (Eq.2) has to be given and the other data, the height, the load carrying capacity and the MISES stresses in the ring as well as in the pipe are determined straightforward by the formulae presented in chapter 3.

## References


[1] EN 1992-1-1, *Design of concrete structures*
[2] EN 1993-1-8, *Design of steel structures, Design of joints*
[3] Guggenberger W., Linder C., *Elastic stress analysis of axisymmetric shells*, ECCS International Conference, Prague, October 2003
[4] Markus G., *Theorie und Berechnung rotationssymmetrischer Bauwerke*, 1976
[5] ABAQUS/Standard, *Abaqus Inc., RI USA*


## Authors


Dr.techn. Robert OFNER, Univ.-Prof. Dr.techn. Richard GREINER
Graz University of Technology, Institute for Steel Structures and Shell Structures
Lessingstrasse 25, A-8010 Graz, AUSTRIA
Phone: +43 316 873 6201, FAX +43 316 873 6707,
E-mail: robert.ofner@tugraz.at, r.greiner@tugraz.at